13C.4 THE IMPACT OF TROPICAL CYCLONES ON MIDLATITUDE ROSSBY WAVE PACKETS: A CLIMATOLOGICAL PERSPECTIVE

Julian F. Quinting*
Karlsruhe Institute of Technology (KIT), Karlsruhe, Germany
Sarah C. Jones
Deutscher Wetterdienst, Offenbach, Germany

1. INTRODUCTION

Tropical cyclones (TCs) that recurve and undergo extratropical transition (ET) (Jones et al., 2003) interact with the midlatitude flow and may modify the extratropical flow pattern in a number of different ways. Recent idealized studies and case studies have shown that this modification can be associated with the amplification or excitation of Rossby waves (Riemer and Jones, 2010; Cordeira and Bosart, 2010; Grams et al., 2011). The dispersion of these Rossby waves into downstream regions has the ability to cause high-impact weather events such as surface cyclogenesis (Agusti-Panareda et al., 2004; Cordeira and Bosart, 2010), cold-air outbreaks (Archambault et al., 2007) and severe precipitation (Martius et al., 2008; Grams et al., 2011). Hence, it is of major interest to investigate the amplification and excitation of Rossby waves as it is an important mechanism by which ET events impact the weather patterns in downstream regions.

Archambault et al. (2013) investigated the interaction between recurving western North Pacific TCs and the midlatitude flow from a climatological perspective for the first time. They stated that such TCs tend to be associated with an amplification of the North Pacific meridional flow pattern. We follow up this statement by investigating the relation between the ET of TCs and the modification of Rossby wave packet (RWP) occurrence frequency and amplitude for three ocean basins from a climatological perspective. Composite maps of eddy kinetic energy budgets are used to investigate key physical processes in cases with and without RWP amplification.

2. DATASET AND METHODOLOGY

In this study, we focus on western North Pacific and South Indian Ocean TCs that recurved and that were designated as extratropical in the period June to November 1980-2010 and December to April 1980-2010, respectively. Six hourly TC positions and the ET-time were retrieved from the IBTrACS database (Knapp et al., 2010). Our RWP identification and analysis of atmospheric fields is based on the European Center for Medium-Range Weather Forecasts (ECMWF) Reanalysis dataset ERA-interim (Dee et al., 2011).

* *Corresponding author address:* Julian F. Quinting, Institute for Meteorology and Climate Research (IMK-TRO), Karlsruhe Institute of Technology (KIT), 76131 Karlsruhe, Germany; e-mail: julian.quinting@kit.edu

RWPs were identified by applying a Hilbert transform filtering technique to the meridional wind (Zimin et al., 2003). The filtering technique eliminates the phase variation in longitude so that the northerly and southerly components of the meridional wind do not cancel out in a composite view. In a comparison of various techniques diagnosing Rossby wave trains, Glatt et al. (2011) stated that a key advantage of the Hilbert transform filtering technique is that once certain thresholds have been chosen large data sets can be screened automatically. Based on this technique, Glatt and Wirth (2013) presented a climatology of Rossby wave trains over the Northern Hemisphere and tested the sensitivity of the technique to the choice of various parameters.

By applying the filtering technique to the meridional wind at 250 hPa along each latitude circle from the equator to the pole we extracted the envelope of the synoptic-scale meridional wind (zonal wavenumber 5 to 15). By concatenating the one-dimensional envelopes for each latitude circle, we obtain the RWP envelope over an entire hemisphere. Afterward, we clip the envelope at a threshold value to identify the RWPs as single objects (Glatt and Wirth, 2013). Finally, we perform a meridional average between 20° and 80°N/S to construct a Hovmöller of the envelope of the meridional wind for consecutive time intervals.

We applied the filtering technique in six-hourly time intervals from seven days prior to ten days after all ET events and created for each TC a Hovmöller diagram as described above. Finally, we made a Hovmöller composite centered on the ET-time of the TCs. In the following, we investigate the mean RWP occurrence frequency F and the mean RWP amplitude $\hat{E}$ defined as

$$F = \frac{1}{N_c} \sum_c M_{i,j}^c \qquad \text{and} \qquad \hat{E} = \frac{\sum_c E_{i,j}^c}{\sum_c M_{i,j}^c} \quad . \qquad (1)$$

N_c denotes the number of cases, $M_{i,j}^c$ is a mask at the grid point i, j in the Hovmöller diagram for case c that is set to 1 if the envelope $E_{i,j}^c > 0$. We determined the statistical significance of the results via a Monte-Carlo approach by creating 1000 random Hovmöller composites of the RWP occurrence frequency and amplitude. Finally, we defined those values of the ET relative composite as statistically significant that either exceed or fall below the upper and lower 5% percentiles of the Monte-Carlo composites. The ET relative composites of synoptic scale RWP occurrence frequency and amplitude are compared to the climatological mean.

3. CLIMATOLOGY OF ROSSBY WAVE PACKETS DOWNSTREAM OF ET EVENTS

3.1 *Western North Pacific ET events*

The RWP occurrence frequency is enhanced significantly downstream of the ET events in the ET relative composite (Fig. 1a). The occurrence frequency exceeds the climatological mean by 15% over the western North Pacific already one day prior to ET. We suggest that this early increase of the RWP occurrence frequency is associated with an approaching trough from upstream and an amplification of the downstream ridge by the outflow of the transitioning TC. The extension of the statistically significant signal in eastward directions with time indicates downstream Rossby wave dispersion. Maximum anomalies in RWP occurrence frequency occur shortly after ET-time. The occurrence frequency in the ET relative composite exceeds the climatological value by more than 20% along 180°E. This maximum is most probably associated with the development of a downstream trough. From one day to five days after ET, a statistically significant enhancement of the RWP occurrence frequency is seen over western and central North America. At some locations the occurrence frequency exceeds the climatological mean by about 10%. The statistical significance and the difference to the climatological mean decrease rapidly along 80°W about five days after the ET events. These results indicate that the impact of TCs on RWPs is limited, in a statistical sense, to the North Pacific and North America. However, it should be noted that cases might exist where the impact of transitioning TCs reaches hemispheric scales.

The RWP amplitude in the ET relative composite is amplified significantly from the Central Pacific to western North America (Fig. 1b). The strongest amplification of more than 1.8 $m\ s^{-1}$ occurs between 180° and 150°W one day after the ET events. This amplification is most likely associated with the development of a downstream trough. The fact that we do not see a strengthening of the RWP amplitude before ET, as we observe it for the RWP occurrence frequency, suggests that the TCs interact with RWPs that are not extraordinarily strong but which are strongly amplified during ET. The difference between the RWP amplitude in the ET relative composite and the climatological mean decreases considerably three days after ET. We suppose that the decrease of the Rossby wave envelope is associated with Rossby wave breaking and the dispersion of kinetic energy.

3.2 *South Indian Ocean ET events*

We applied the same method to all ET events over the western South Indian Ocean in the period 1980 to 2010. The RWP occurrence frequency is significantly amplified by 12 to 15% downstream of the ET events over the South Indian Ocean (Fig. 2a). However, the observed signal is not as strong as for the western North Pacific TCs (Fig. 1a). The RWP occurrence frequency starts to increase significantly one day prior to ET in the vicinity

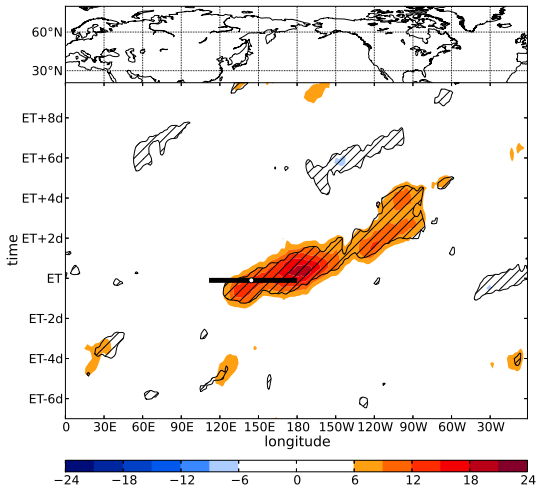

(a) Anomaly in RWP occurrence frequency [%]

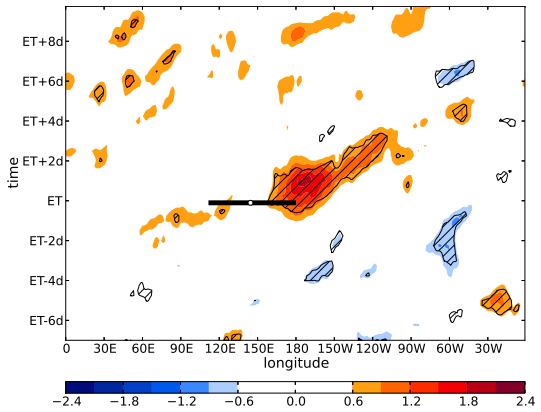

(b) Anomaly in RWP amplitude [$m\ s^{-1}$]

FIG. 1: Anomaly of RWP occurrence frequency [%] (a) and RWP amplitude [$m\ s^{-1}$] (b) from June to November climatology for western North Pacific TCs. Values that are statistically significant at the 95% confidence level are hatched. Black horizontal bar marks the range of longitudes of TCs at ET-time. White circle marks the mean longitude of all TCs at ET-time. 280 cases were used.

of the ET events. The statistically significant signal persists for three days and decreases over Australia. A further only partially statistically significant increase in RWP occurrence frequency can be observed over the western South Pacific later. The RWP occurrence frequency is enhanced by 6 to 12% compared to the climatological value two to four days after the ET events.

The RWP amplitude enhancement is as strong as over the western North Pacific. It is amplified by more than 1.8 $m\ s^{-1}$ between 90° to 150°E from one to five days after the ET events (Fig. 2b). A second region with an amplified RWP amplitude can be found between 150°E to 150°W from three to seven days after ET. The amplification of the RWP amplitude and an increase in occurrence frequency in this region indicates the development of a further downstream trough over the west-

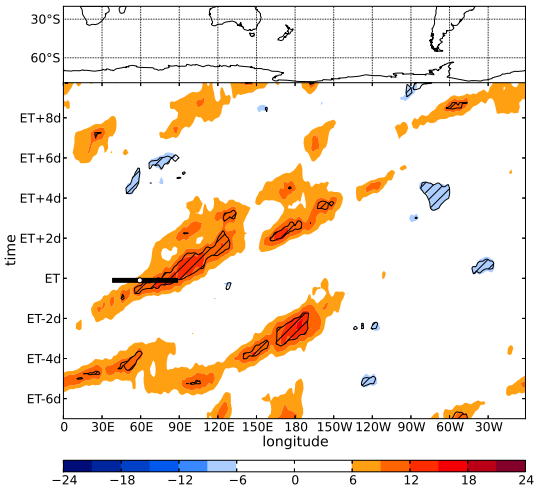

(a) Anomaly in RWP occurrence frequency [%]

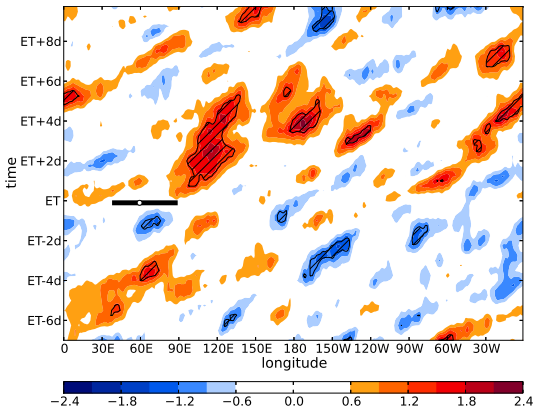

(b) Anomaly in RWP amplitude [$m\ s^{-1}$]

FIG. 2: As in Fig. 1 for anomaly from December to April climatology for the western South Indian Ocean TCs. 114 cases were used.

ern South Pacific after ET events. The decrease of the RWP amplitude and occurrence frequency over eastern Australia three days after ET is indicative of Rossby wave breaking.

3.3 *North Atlantic ET events*

RWP occurrence frequency and amplitude do not increase statistically significant downstream of North Atlantic ET events (not shown). Since the climatological RWP occurrence frequency and amplitude are high over the western North Atlantic, ET events in this region do not impact RWP in a statistical sense. We suggest that most of the TCs interact with RWPs emerging from North America without triggering new RWPs. Nevertheless, case studies have highlighted the impact of northern Atlantic TCs on the midlatitude flow (e. g. Agusti-Panareda et al., 2004; Grams et al., 2011). This indicates that TCs in this region are able to modify RWPs but that modifications do not differ significantly from the general variability.

4. COMPOSITE ANALYSIS OF CASES WITH AND WITHOUT ROSSBY WAVE DEVELOPMENT

4.1 *Identification of cases*

We identified cases with and without downstream Rossby wave development after the western North Pacific ET events. By doing so, we are able to make a classification based on the downstream flow response independently of the structure of the TC. This type of classification complements the study by Archambault et al. (2013) who distinguished between two scenarios based on a TC-midlatitude flow interaction metric.

In order to distinguish between the two cases we generated a mask. This mask is defined by the 90% confidence level of the Monte-Carlo approach between 90°E to 140°W and from two days prior to three days after ET. Afterward, we determined the area in this mask that exhibits a RWP amplitude greater than zero for each case. The quintiles of cases that fill the largest/smallest area of the mask are in the following defined as Rossby wave case (RW case)/no Rossby wave case (noRW case). Each quintile consists of 56 ET events.

A precursor Rossby wave emanates from the Asian continent in the RW case (Fig. 3a). About three days prior to the ET event a weak ridge exists over eastern Asia at 90°E. It is followed by a downstream trough with its axis located about 15°W of the approaching TC at ET-time. The TC itself is collocated with the eastern flank of this trough which is strongly amplified prior to ET-time. This amplification indicates the interaction between the transitioning TC and the midlatitude flow. A typical Rossby wave train pattern develops downstream of the ET events. It can be traced to central North America. The Rossby wave train signal decreases about three days after the ET events over that region. In the cases without a Rossby wave development a precursor wave train can not be observed (Fig. 3b). A weak ridge starts to develop between 120° and 150°E about two days prior to ET. It reaches its peak intensity at ET-time which suggests that the ET system acts as a local source of eddy kinetic energy leading to an amplification of the meridional wind. However, the ridge vanishes already two days after ET and a further downstream development can not be observed.

The observed pattern suggests that a precursor Rossby wave emanating from the Asian continent favors the conditions for a Rossby wave development over the North Pacific after ET events. However, the existence of a precursor Rossby wave does not necessarily result in a strong downstream development. Several previous studies showed that the downstream flow amplification also strongly depends on the phasing between the transitioning TC and the midlatitude flow.

4.2 *Composite analysis of Eddy Kinetic Energy Budgets*

Recent studies have shown that TCs may act as an additional eddy-kinetic-energy (K_e) source to the midlatitude flow (Harr and Dea, 2009; Keller et al., 2014; Keller and

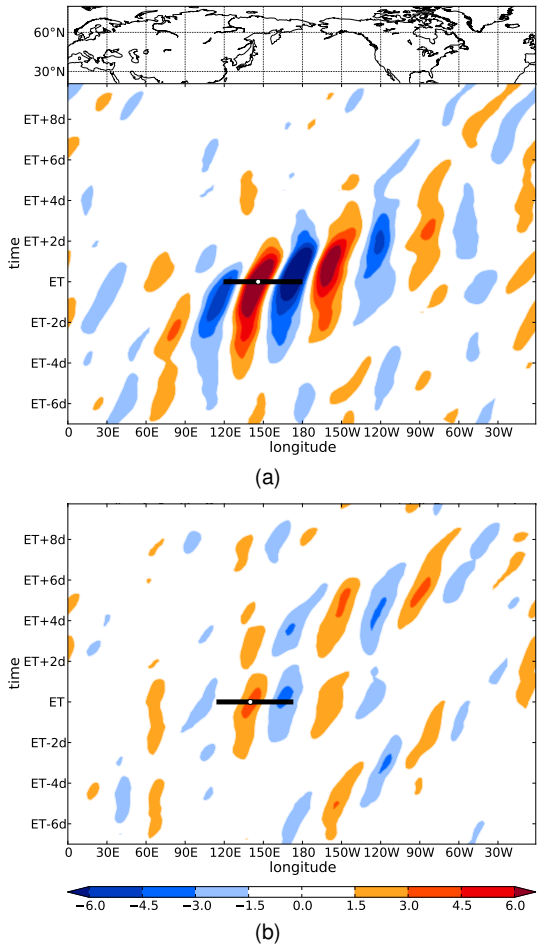

FIG. 3: Meridional wind for zonal wave number 5 to 15 at 250 hPa averaged between 20° and 80°N centered on mean TC position at ET-time. RW case (a) and noRW case (b). Black horizontal bar marks the range of longitudes of TCs at ET-time. White circle marks the mean longitude of all TCs at ET-time.

Grams, 2014). To investigate a possible impact of the TCs on the wave amplification in the RW cases, we calculated a K_e-budget composite centered on the mean TC position and compared this to a K_e-budget composite for the noRW cases. According to Orlanski and Sheldon (1995), the energy budget is divided into the sum of a time mean part (subscript $_m$) and a perturbation part. The mean is defined as a 30-day running mean centered around each best track time step of the individual TCs. The time tendency of $K_e = \frac{1}{2}|\mathbf{v}|^2$ is defined in pressure coordinates as

$$\frac{\partial K_e}{\partial t} = -(\mathbf{v}\cdot\nabla_p\phi) - [\nabla_p\cdot(\mathbf{V}K_e)] - \frac{\partial(\omega K_e)}{\partial p} - \mathbf{v}\cdot(\mathbf{v}\cdot\nabla_p\mathbf{V}_m) + \textit{Residue} \quad (2)$$

ϕ denotes the geopotential height perturbation and ∇_p the horizontal gradient operator. The second and third term on the right-hand side (RHS) of (2) are the horizontal and vertical divergence of the K_e fluxes. The fourth term on the RHS defines the barotropic generation of K_e. The first term on the RHS of (2) represents the generation of K_e and is defined as

$$-\mathbf{v}\cdot\nabla_p\phi = -\nabla_p\cdot(\mathbf{v}\phi)_a - \omega\alpha - \frac{\partial(\omega\phi)}{\partial p} \quad (3)$$

The first term on the RHS in (3) is the ageostrophic (subscript $_a$) geopotential flux divergence and describes the dispersion of kinetic energy. The second term represents the baroclinic conversion from available eddy potential energy to K_e. The last term is the vertical flux divergence which is negligible since we consider vertical integrals between 1000 and 100 hPa.

Three centers of K_e exist in the RW case composite 24 hours prior to ET (Fig. 4a). The first K_e center is associated with the transitioning TC at 32°N and 138°E. A second K_e center is located on the eastern flank of the upstream trough and a third K_e center exists in downstream regions. In the noRW case, a weak midlatitude K_e center develops to the northeast of the TC (Fig. 4b) in the crest of the weak downstream ridge.

The baroclinic conversion from potential into K_e exhibits remarkable differences between the two scenarios. In the noRW case the baroclinic conversion exhibits largest values to the north and northeast of the TC (Fig. 4b). In the RW case the baroclinic conversion is much stronger and extends over a broader region (Fig. 4a). This indicates strong lifting of warm air masses in the vicinity of the TC and north of it along the baroclinic zone.

In both scenarios, divergence of the ageostrophic geopotential flux compensates the baroclinic conversion term (Fig. 4c, 4d). Strong divergence of the ageostrophic geopotential flux indicates the dispersion of baroclinically produced K_e into the midlatitudes in both scenarios. In the noRW case, weak convergence of the ageostrophic geopotential flux in the crest of the weak downstream ridge indicates accumulation of K_e (Fig. 4d). The ageostrophic geopotential flux vectors suggest that the ageostrophic geopotential flux convergence results from the merging of the subtropical and polar jet to the north of the TC. Much stronger convergence of the ageostrophic geopotential flux can be found in the RW case (Fig. 4c). A convergence of the ageostrophic flow between the upstream trough and the TC outflow leads to a strong accumulation of K_e. This results primarily in an amplification of the meridional flow in the western flank of the downstream ridge. This stands in contrast to the noRW cases where the accumulation of K_e through ageostrophic geopotential flux convergence amplifies the flow in the crest of the ridge. A further amplification of the meridional flow component can be found downstream in the RW case where convergence of the ageostrophic geopotential fluxes leads to accumulation of K_e in the flank of the developing midlatitude trough.

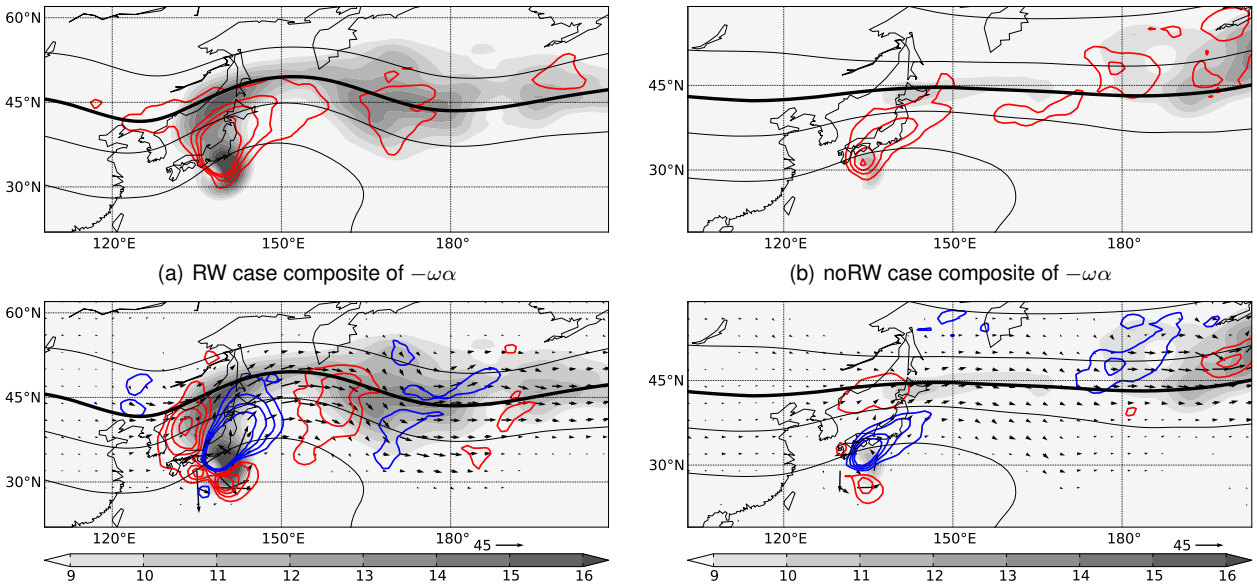

(a) RW case composite of $-\omega\alpha$

(b) noRW case composite of $-\omega\alpha$

(c) RW case composite of $-\nabla_p \cdot (\mathbf{v}\phi)_a$

(d) noRW case composite of $-\nabla_p \cdot (\mathbf{v}\phi)_a$

FIG. 4: Composite maps of K_e budget terms centered on the mean TC position for the RW case (a, c) and the noRW case (b, d) one day prior to ET-time. (a, b) vertically averaged K_e (shaded, 10^5 J m^{-2}), 200 hPa geopotential heights (contours, 2000 m^2 s^{-2} intervals, thick black line illustrates 118000 m^2 s^{-2} isoline) and vertically averaged K_e generation resulting from baroclinic conversion (contours, contour interval 8 W m^{-2}). (c, d) as in (a, b), but for the vertically averaged K_e resulting from geopotential flux convergence, ageostrophic geopotential flux vectors (reference vector in lower right, 10^6 W m^{-1}).

5. SUMMARY

This study presents a climatological investigation of the impact of TCs on midlatitude RWPs. We identified RWPs that occurred from seven days before to ten days after the ET events in three ocean basins during the period 1980 to 2010. We identified RWPs via the Hilbert transform of the meridional wind at 250 hPa (Zimin et al., 2003). This method enabled us to identify RWPs as objects so that we could determine their occurrence frequency and amplitude.

We found a statistically significant increase in RWP amplitude and occurrence frequency associated with ET events over the western North Pacific (Fig. 1). In the ET relative composite, the RWP occurrence frequency exceeds the climatological mean by up to 20% between 120°E and 80°W from one day prior to four days after the ET events. The strongest anomaly occurs over the central North Pacific. But even over North America the RWP occurrence frequency exceeds the climatological mean by more than 12%. The statistically significant RWP amplitude increases by up to 2 m s^{-1} between 160°E and 110 °W from ET-time to four days after ET. The observed amplification of the meridional flow is consistent with results of Archambault et al. (2013) who found an increase of the North Pacific flow pattern downstream of ET.

South Indian Ocean TCs that undergo ET have a statistically significant impact on RWPs, also (Fig. 2). However, the deviations from the climatological mean are not as strong as over the western North Pacific. The RWP occurrence frequency exceeds the climatological mean by up to 15% between 60° and 130°E from one day prior to ET to two days after ET. The strongest anomaly occurs over the eastern South Indian Ocean about one day after ET. Over the same region, the RWP amplitude is enhanced considerably by up to 2 m s^{-1}.

In order to identify synoptic conditions and physical processes that favor the development of RWPs downstream of ET events we investigated the downstream response to western North Pacific ET events in a composite view. Therefore, we determined the strength of the Rossby wave signal downstream of each TC. We chose the upper and lower quintile of all ET events to be representative of cases with and without downstream Rossby wave development. A Hovmöller diagram of the meridional wind suggests that a precursor Rossby wave that emerges from the Asian continent favors the conditions for a Rossby wave train downstream of the ET events (Fig. 3). The precursor Rossby wave is strongly amplified during the interaction with the TC and disperses over the North Pacific toward North America. These results coincide with findings of Riemer and Jones (2010). They concluded that the leading edge of a developing baroclinic wave represents an optimal location where an ET system can impact the downstream flow most significantly.

We created composite maps of K_e budget terms for the RW and noRW cases to assess the impact of the TCs on the wave amplification. K_e that is generated through

baroclinic conversion in the vicinity of the transitioning TCs, is dispersed via divergence of the ageostrophic geopotential flux (Fig. 4). Strong ageostrophic geopotential flux convergence contributes to the development of a primary midlatitude K_e center on the eastern flank of the trough upstream of the TC in the RW cases. The accumulation of K_e results from the convergence of the midlatitude flow and the TC outflow. This convergence indicates that the TC provides additional K_e to the midlatitude flow and contributes to the Rossby wave amplification. Once a midlatitude K_e center has developed, K_e is dispersed through div- and converging ageostrophic geopotential fluxes into downstream regions where it contributes to the formation of further K_e centers in the flanks of the developing troughs and ridges. These findings coincide with results from Harr et al. (2000), Harr and Dea (2009) and Keller et al. (2014). In the noRW cases the ageostrophic geopotential flux convergence between the TC outflow and the midlatitude flow associated with the upstream trough does not occur. Therefore, a K_e center does not develop in the eastern flank of the upstream trough. Instead, convergence of ageostrophic fluxes due to the merging of the split jet leads to an accumulation of K_e in the crest of the downstream ridge. This accumulation leads to the acceleration of the midlatitude jet but not to an amplification of the RWPs.

Acknowledgments

This project was supported by the German Research Foundation (DFG) as part of the research unit PANDOWAE (FOR896).

REFERENCES

Agusti-Panareda, A., C. D. Thorncroft, G. C. Craig, and S. L. Gray, 2004: The extratropical transition of hurricane Irene (1999): A potential-vorticity perspective. *Quart. J. Roy. Meteor. Soc.*, **130**, 1047–1074.

Archambault, H. M., L. F. Bosart, and D. Keyser, 2007: Recurving typhoons as precursors to an early season arctic outbreak over the continental U.S. *Ninth Northeast Regional Operational Workshop*, Albany, NY, National Weather Service/Amer. Meteor. Soc., 1–55, [Available online at http://cstar.cestm.albany.edu/nrow/nrow9/Archambault/archambault. ppt.].

Archambault, H. M., L. F. Bosart, D. Keyser, and J. M. Cordeira, 2013: A climatological analysis of the extratropical flow response to recurving western north pacific tropical cyclones. *Mon. Wea. Rev.*, **141**, 2325–2346.

Cordeira, J. M. and L. F. Bosart, 2010: The antecedent large-scale conditions of the "Perfect Storms" of late October and early November 1991. *Mon. Wea. Rev.*, **138**, 2546–2569.

Dee, D. P., et al., 2011: The ERA-Interim reanalysis: configuration and performance of the data assimilation system. *Q. J. R. Meteorol. Soc.*, **137**, 553–597.

Glatt, I., A. Dörnbrack, S. Jones, J. Keller, O. Martius, A. Müller, D. H. W. Peters, and V. Wirth, 2011: Utility of Hovmöller diagrams to diagnose Rossby wave trains. *Tellus A*, **63**, 991–1006.

Glatt, I. and V. Wirth, 2013: Identifying Rossby wave trains and quantifying their properties. *Q. J. R. Meteorol. Soc.*, doi: 10.1002/qj.2139.

Grams, C. M., et al., 2011: The key role of diabatic processes in modifying the upper-tropospheric wave guide: a North Atlantic case-study. *Quart. J. Roy. Meteor. Soc.*, **137**, 2174–2193.

Harr, P. A. and J. M. Dea, 2009: Downstream Development Associated with the Extratropical Transition of Tropical Cyclones over the Western North Pacific. *Mon. Wea. Rev.*, **137**, 1295–1319.

Harr, P. A., R. L. Elsberry, and T. F. Hogan, 2000: Extratropical Transition of Tropical Cyclones over the Western North Pacific. Part II: The Impact of Midlatitude Circulation Characteristics. *Mon. Wea. Rev.*, **128**, 2634–2653.

Jones, S. C., et al., 2003: The extratropical transition of tropical cyclones: Forecast challenges, current understanding, and future directions. *Wea. Forecasting*, **18**, 1052–1092.

Keller, J. and C. M. Grams, 2014: The Extratropical Transition of Typhoon Choi-Wan (2009) and its impact on high-impact weather events in North America. *Mon. Wea. Rev.*, **submitted**.

Keller, J., S. C. Jones, and P. A. Harr, 2014: An eddy kinetic energy view of physical and dynamical processes in distinct forecast scenarios for the extratropical transition of two tropical cyclones. *Mon. Wea. Rev.*, **submitted**.

Knapp, K. R., M. C. Kruk, D. H. Levinson, H. J. Diamond, and C. J. Neumann, 2010: The International Best Track Archive for Climate Stewardship (IBTrACS). *Bull. Amer. Meteor. Soc.*, **91**, 363–376.

Martius, O., C. Schwierz, and H. C. Davies, 2008: Far-upstream precursors of heavy precipitation events on the Alpine south-side. *Quart. J. Roy. Meteor. Soc.*, **134**, 417–428.

Orlanski, I. and J. P. Sheldon, 1995: Stages in the energetics of baroclinic systems. *Tellus A*, **47**, 605–628.

Riemer, M. and S. C. Jones, 2010: The downstream impact of tropical cyclones on a developing baroclinic wave in idealized scenarios of extratropical transition. *Q. J. R. Meteorol. Soc.*, **136**, 617–637.

Zimin, A. V., I. Szunyogh, D. J. Patil, B. R. Hunt, and E. Ott, 2003: Extracting Envelopes of Rossby Wave Packets. *Mon. Wea. Rev.*, **131**, 1011–1017.